Progress In Electromagnetics Research M, Vol. 109, 241–251, 2022

Model Predictive Current Control of Permanent Magnet Synchronous Motor for Marine Electric Propulsion

Xiyang Zhao, Jingwei Zhu*, and Zhibin Wang

Abstract—In order to solve high torque ripple of permanent magnet synchronous motor (PMSM) for marine electric propulsion under the current control methods, the improved model predictive current control (MPCC) of PMSM for marine electric propulsion based on the mathematical model of three-phase PMSM is proposed. First, the stator current prediction model is derived based on the forward Euler method. Then the first optimal voltage vector is obtained by the value function, and the second optimal voltage vector, and the second optimal voltage vector and the first and second optimal voltage vectors' respective action times are obtained by the q-axis deadbeat control, which are directly fed back to the inverter. The proposed control method is verified by simulation and hardware in the loop simulation experiment. The experiment results show that in comparison with the direct torque control based on space vector modulation (SVM-DTC) in the case of motor speed and torque mutation, the torque ripple of motor is reduced by 9.40% and 4.80% respectively based on improved MPCC. The feasibility and effectiveness of the proposed method are verified by the simulation and experiment results.

1. INTRODUCTION

Marine electric propulsion system has broad application prospects due to its merits of strong driving ability, convenient installation, and maintenance [1–3]. Permanent magnet synchronous motor (PMSM) has been widely used as propulsion motor due to its wide speed regulation range, low noise, and high power density [4–6].

Propulsion motor drive control technology has been highly concerned by scholars as the core technology of marine electric propulsion system [7, 8]. A current hysteresis vector control method for ship propulsion motor is proposed in [9], but this method has the problem of large electromagnetic torque ripple. A direct torque control (DTC) method of multi hysteresis torque regulator for PMSM in marine electric propulsion system is proposed in [10–12], which has been a research hot spot of marine electric propulsion motor control method owing to simple control structure and good dynamic response performance. However, direct torque control method of multi hysteresis torque regulator has a problem that its output electromagnetic torque ripple is large, which leads to poor motor stability and large mechanical noise.

Therefore, reducing the torque ripple of PMSM for marine electric propulsion has become a hot spot of researchers. A three-level inverter control technology based on the PMSM direct torque control of electric propulsion is proposed in [13, 14] to make flux and torque more stable. However, three-level inverter has many problems, such as neutral point voltage balance, the cost of hardware, and the complexity of control. A control method of dividing stator flux into 12 sectors and adding zero voltage vector based on the traditional direct torque control is proposed in [15], so as to reduce the electromagnetic torque ripple of the motor. In order to reduce the torque ripple of motor, the

Received 10 February 2022, Accepted 31 March 2022, Scheduled 15 April 2022
* Corresponding author: Jingwei Zhu (zjwdl@dlmu.edu.cn).
The authors are with the College of Marine Electrical Engineering, Dalian Maritime University, Dalian 116026, China.

direct torque control based on space vector modulation (SVM-DTC) is proposed in [16, 17], which takes induction motor as an example. The SVM-DTC based on three-level inverter for electric propulsion PMSM is proposed in [18], which improves the performance of starting and speed regulation. Taking the marine PMSM as the research object, a control method that adds the fuzzy logic control algorithm based on DTC is proposed in [19], which uses a fuzzy controller to replace the traditional hysteresis torque controller, so as to realize the low ripple effect of torque and flux. However, the control method is complex which leads to large amount of calculation and the difficult implementation. Model predictive torque control (MPTC) taking the ship propulsion motor as the control object is proposed in [20]. It reduces the electromagnetic torque ripple. In addition, it is more suitable for the ship electric propulsion system with complex working environment due to its multi constraint processing ability and nonlinear processing ability, but its tuning procedure is complex because the cost function of MPTC includes weight coefficient.

In order to solve the problem of large torque ripple in the traditional control method of PMSM for marine electric propulsion, an improved model predictive current control (MPCC) of PMSM for marine electric propulsion is proposed in this paper, which reduces the electromagnetic torque ripple of the motor and improves the multi constraint processing ability of the control system. The effectiveness of the proposed control strategy is verified by MATLAB/Simulink simulation and hardware in the loop simulation experiments.

2. MATHEMATICAL MODEL OF PMSM

The surface mounted permanent magnet synchronous motor (SPMSM) stator voltage equation in d-q coordinate system can be expressed as:

$$\begin{cases} u_d = R_s i_d + L_s \dfrac{di_d}{dt} - \omega_e L_s i_q \\ u_q = R_s i_q + L_s \dfrac{di_q}{dt} + \omega_e \left(L_s i_d + \psi_f\right) \end{cases} \tag{1}$$

where u_d and u_q are voltage components in d- and q-axes, respectively; i_d and i_q are current components in d- and q-axes, respectively; L_s and R_s are the inductance of stator and the resistance of stator, respectively; ω_e is the electrical angular velocity of the rotor; ψ_f is the flux linkage of permanent magnet.

The stator current differential equation of SPMSM in d-q coordinate system can be derived from Equation (1):

$$\begin{cases} \dfrac{di_d}{dt} = \dfrac{1}{L_s}\left(u_d - R_s i_d + \omega_e L_s i_q\right) \\ \dfrac{di_q}{dt} = \dfrac{1}{L_s}\left(u_q - R_s i_q - \omega_e L_s i_d - \omega_e \psi_f\right) \end{cases} \tag{2}$$

The electromagnetic torque equation of the SPMSM is shown as:

$$T_e = \frac{3}{2} p_n i_q \psi_f \tag{3}$$

where T_e is the electromagnetic torque of the motor; P_n is the pole pairs of the motor.

3. IMPROVED MODEL PREDICTIVE CURRENT CONTROL STRATEGY OF PMSM

3.1. Principle of Improved Model Predictive Current Control Strategy

A two-level inverter is used to drive the three-phase SPMSM in this paper, which produces 8 switching states including 6 effective voltage vectors and 2 zero voltage vectors. Space voltage vector diagram of two-level inverter is shown in Figure 1, where "0" represents the conduction of the lower bridge arm, and "1" represents the conduction of the upper bridge arm.

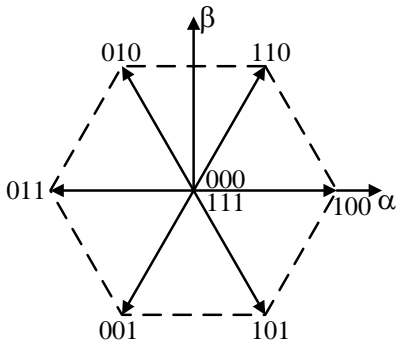

Figure 1. Space voltage vector diagram of two-level inverter.

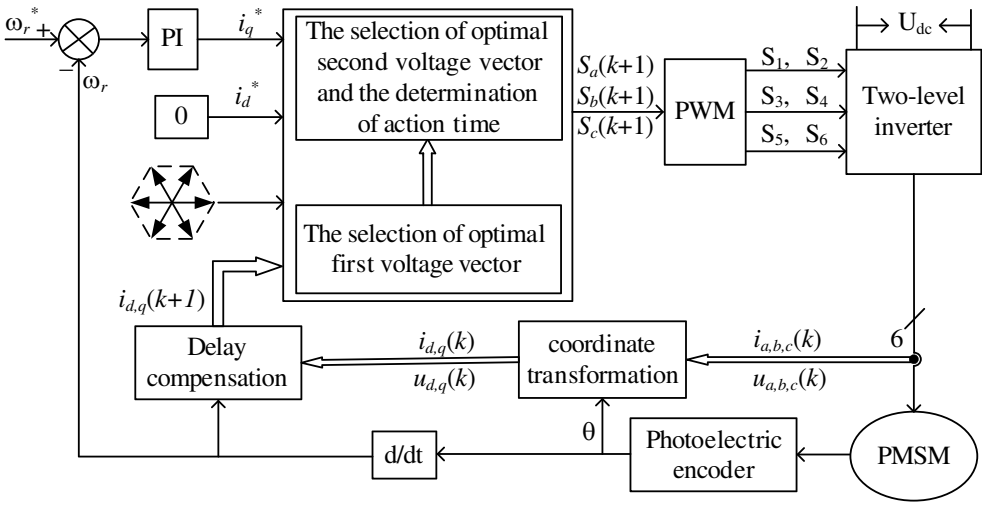

Figure 2. The structure block diagram of PMSM control system based on improved MPCC.

The structure block diagram of SPMSM control system based on improved MPCC is shown in Figure 2. Firstly, a PI controller is used to convert the speed difference into the torque current reference value i_q^*, and the improved MPCC method is used in the current loop to track the reference current. Meanwhile, in each sampling period, the predicted current formula is used for delay compensation and stator current prediction under the 8 voltage vectors, and then the optimal first voltage vector u_{opt1} is determined by the cost function. Then, 8 voltage vectors are used as the second alternative voltage vector. And the optimal second voltage vectors u_{opt2}, the action time t_{opt1} of the optimal first voltage vector u_{opt1} and the action time t_{opt2} of the optimal second voltage vector u_{opt2} are obtained which use q-axis deadbeat control, predictive current formula, and cost function, and then the PMSM is controlled.

Equation (2) is discretized by the forward Euler method, and the next time prediction model of d-axis and q-axis stator currents can be obtained as:

$$\begin{cases} i_d(k+1) = \left(1 - \dfrac{T_s}{L_s}R_s\right) i_d(k) + \dfrac{T_s}{L_s}\omega_e(k)L_s i_q(k) + \dfrac{T_s}{L_s}u_d(k) \\ i_q(k+1) = \left(1 - \dfrac{T_s}{L_s}R_s\right) i_q(k) + \dfrac{T_s}{L_s}\omega_e(k)L_s i_d(k) + \dfrac{T_s}{L_s}u_q(k) - \dfrac{T_s}{L_s}\omega_e(k)\psi_f \end{cases} \tag{4}$$

where k is the current time; $k+1$ is the next time; T_s is the sampling period.

$u_d(k)$ and $u_q(k)$ are substituted into the current prediction formula to obtain the predicted current value at the next time. In order to eliminate the one beat delay of the digital control system, the obtained predicted current value is taken as the initial known quantity. And substitute the obtained

predicted current value and 8 voltage vectors into the current prediction formula to obtain 8 groups in d- and q-axis predicted current values at the next moment after compensation, which are substituted into the cost function, respectively. Finally, the corresponding voltage vector is selected as u_{opt1} to minimize the cost function, and the cost function used in this paper is obtained as:

$$g_z = |i_d^* - i_d(k+1)| + \left|i_q^* - i_q(k+1)\right| \tag{5}$$

where i_d^* and i_q^* are the given value components of stator current in d- and q-axes, respectively.

According to the q-axis deadbeat control, the predicted value of q-axis stator current is equal to the given value of q-axis stator current:

$$\begin{cases} i_q^* = i_q(k+1) = i_q(k) + f_{opt1}t_{opt1}^* + f_{opt2}t_{opt2}^* \\ T_s = t_{opt1}^* + t_{opt2}^* \end{cases} \tag{6}$$

where f_{opt1} and f_{opt2} are the slope of q-axis current component change under the action of f_{opt1} and the second alternative voltage vector, respectively, and the calculation formula is shown as follows:

$$\begin{cases} f_{opt1} = f_0 + \dfrac{u_{q\_opt1}}{L_s} \\ f_{opt2} = f_0 + \dfrac{u_{q\_opt2}}{L_s} \\ f_0 = \dfrac{1}{L_s}\left(-R_s i_q - \omega_e L_s i_d - \omega_e \psi_f\right) \end{cases} \tag{7}$$

where u_{q_opt1} and u_{q_opt2} are the q-axis component of the optimal first voltage vector and the q-axis component of the second alternative voltage vector, respectively.

Combining Equations (6) and (7), the expressions of t_{opt1}^* and t_{opt2}^* can be obtained as:

$$\begin{cases} t_{opt1}^* = \dfrac{i_q^* - i_q(k) - f_{opt2}T_s}{f_{opt1} - f_{opt2}} \\ t_{opt2}^* = T_s - t_{opt1}^* \end{cases} \tag{8}$$

Taking 8 voltage vectors as the second alternative voltage vectors and substituting them into Equations (6) and (8) respectively to obtain t_{opt1}^* and t_{opt2}^* under different alternative voltage vectors, then 8 sets of synthetic voltage vectors can be obtained by Equation (9):

$$u_{dqj} = u_{opt1}\frac{t_{opt1j}^*}{T_s} + uj_{opt2}\frac{t_{opt2j}^*}{T_s} \tag{9}$$

where $j = 1, 2, \ldots, 8$.

Using the 8 sets of synthetic voltage vectors substituted into the prediction current formula (4) can obtain the corresponding current prediction value at next time. Finally, the voltage vector corresponding to minimizing the cost function is selected as u_{opt2}. The two-level inverter is controlled according to the obtained u_{opt1} and u_{opt2} and their corresponding action times t_{opt1} and t_{opt2}, and then the PMSM is controlled.

3.2. Flowchart of Improved Model Predictive Current Control Strategy

The flowchart of the improved MPCC strategy is shown in Figure 3. Firstly, the sampling information is obtained, including the rotor position θ of PMSM by photoelectric encoder; the actual speed ω_r of PMSM is obtained by differential treatment of θ; the stator current components $i_d(k)$ and $i_q(k)$ of d- and q-axes at time k of PMSM are obtained; the output voltage components $u_d(k)$ and $u_q(k)$ of d- and q-axes at time k of two-level inverter are obtained. Then, the optimal first voltage vector u_{opt1} is calculated according to Equations (4) and (5). Finally, the optimal second voltage vectors u_{opt2}, the action time t_{opt1} of the optimal first voltage vector u_{opt1}, and the action time t_{opt2} of the optimal second voltage vectors u_{opt2} are obtained according to q-axis deadbeat control and Equations (4) to (9). Then, the normal operation of the PMSM is controlled.

g_{opt1} and g_{opt2} are the cost functions when the optimal first voltage vector and optimal second voltage vector are selected, respectively; f_j is the slope of the q-axis current component of the second voltage vector when different alternative voltage vectors are selected.

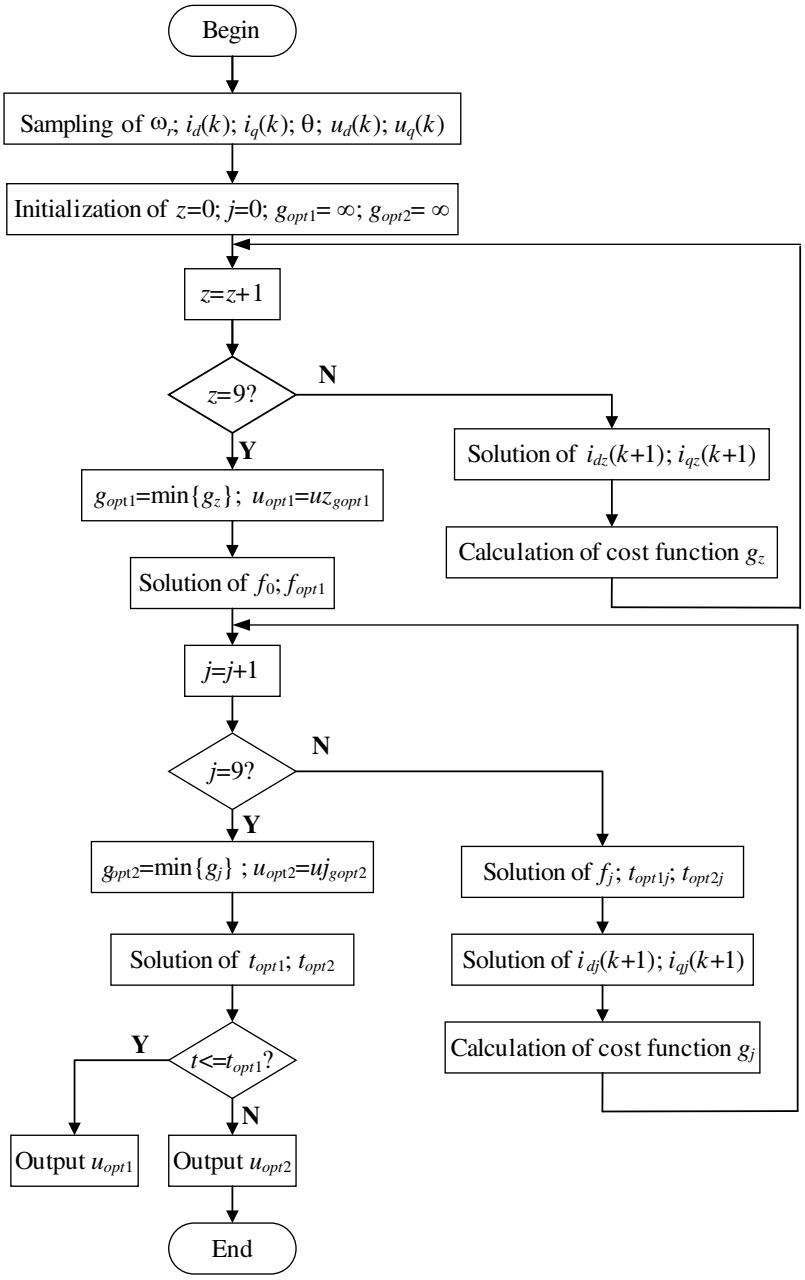

Figure 3. Flow chart of improved MPCC strategy.

4. SIMULATION VERIFICATION

In order to verify the effectiveness of the proposed method, the simulation model of the improved MPCC of PMSM for marine electric propulsion is built in MATLAB/Simulink, and compared with the simulation results of PMSM for marine electric propulsion control system based on SVM-DTC. In order to ensure that the simulation effect is more in line with the practical application of electronic devices in reality, the sampling frequency of the simulation model is set as 10 kHz. To compare the performance of the two control methods, the torque ripple is defined as:

$$T_{\text{ripple}} = \frac{\max\left\{\left|T_{\max} - T_{avg}\right|, \left|T_{\min} - T_{avg}\right|\right\}}{T_{avg}} \tag{10}$$

In the model, the main parameters of the SPMSM which is used as the electric propulsion motor are shown in Table 1.

Table 1. Parameters of SPMSM.

Motor parameters	Value
Rated power P_n/kW	4088
Rated voltage U_n/V	1800
Rated speed n/(r/min)	200
Rated torque T_n/(kNm)	195.2
Stator inductance L_s/μH	476.7
Pole-pair numbers P_n	8
Moment of inertia J/(kgm^2)	550
Rotor flux linkage ψ_f/wb	3.55
Stator resistance R_s/Ω	0.1502

4.1. Speed Mutation Simulation

In order to simulate the actual operation condition and prevent the overcurrent during the starting process, the motor is started under no-load condition, and the reference speed is set as three stages. The initial reference speed is 60 r/min, then the given speed is increased to 90 r/min and 120 r/min at 0.75 s and 1.25 s, respectively. The load torque of 97.6 kNm is applied to the motor at 0.25 s.

The motor response curves of the PMSM control system with SVM-DTC and improved MPCC under the variable speed condition are shown in Figure 4(a) and (b), respectively. The simulation results show that the torque ripple is 14.44% with the SVM-DTC, and the torque ripple is 8.05% with the improved MPCC under the same simulation conditions. Therefore, the torque ripple of the PMSM control system with the improved MPCC can be reduced compared with SVM-DTC in the case of motor speed variation.

4.2. Load Mutation Simulation

The given initial speed is set as 120 r/min, motor start with no-load. The load increases to 97.6 kNm at 0.25 s at the stably running period. The load rises to rated load 195.2 kNm at 0.75 s when the motor is stable again. The load drops to half load 97.6 kNm at 1.25 s when the motor is stable again until the end of simulation.

The motor response curves of the PMSM control system with SVM-DTC and improved MPCC under the variable load condition are shown in Figure 5(a) and (b), respectively. It can be calculated from the simulation that the torque ripples with the SVM-DTC and improved MPCC are 7.39% and 4.28%, respectively, when the load is suddenly changed until the motor runs stably. Therefore, the torque ripple of the PMSM control system with the improved MPCC can be reduced compared with SVM-DTC in the case of motor load variation.

The results of simulation experiment show that in comparison with the SVM-DTC under the same simulation conditions, the torque ripple is reduced by 6.39% and 3.11%, respectively, in the cases of motor speed and torque mutation for the proposed method in the paper.

5. EXPERIMENTAL VERIFICATION

Due to the large power of the motor studied in this paper, it is difficult to use the prototype motor for hardware experiment, so the StarSim hardware in the loop simulation platform is used for experimental verification. The experimental platform is shown in Figure 6, and it includes hardware in the loop (HIL)

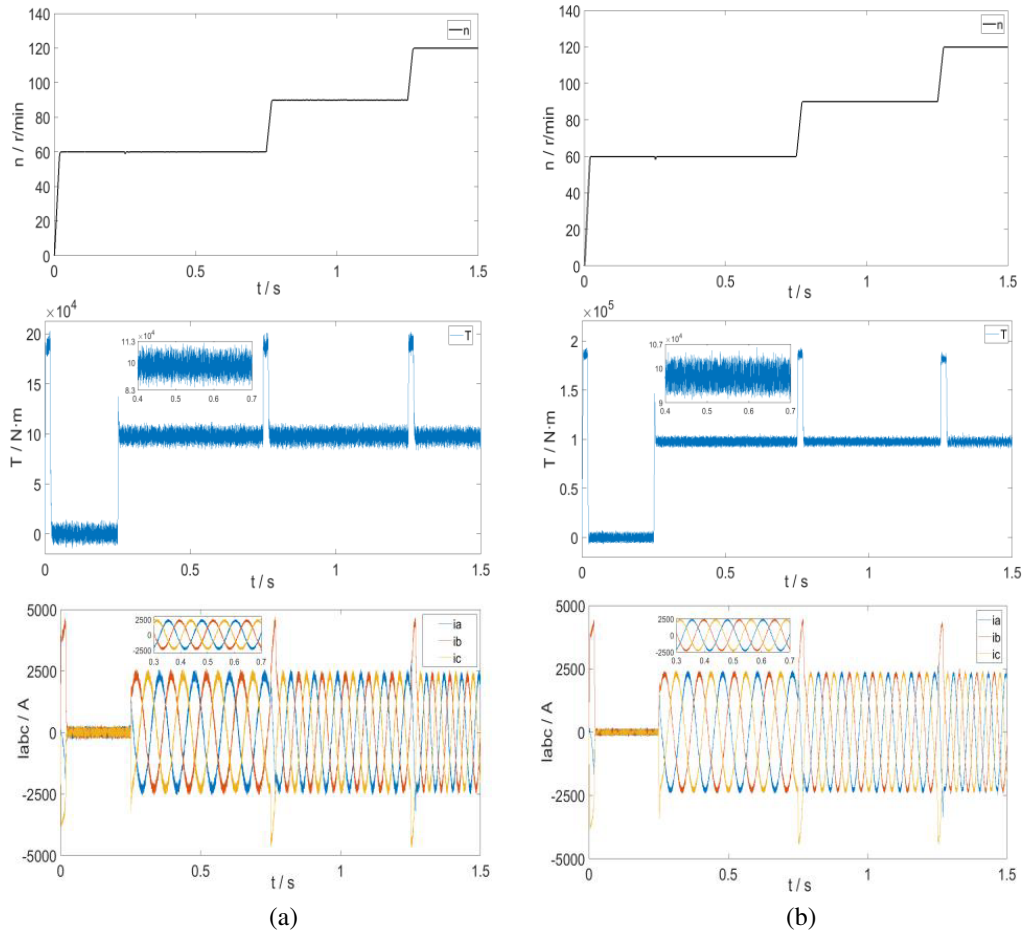

Figure 4. The motor response curves of the PMSM control system based on (a) SVM-DTC and (b) improved MPCC.

and rapid control prototyping (RCP). The communication between RCP and HIL depends on the IO channel connected to the I/O board [21, 22]. The motor model and main power circuit model are built on HIL. RCP is used to detect the three-phase current, torque, rotor position, and other signals output by HIL, and complete the implementation function of improved MPCC strategy. The motor parameters used in the experiment are consistent with those in MATLAB simulation. The sampling frequency of hardware in the loop simulation control system is 10 kHz. The speed, d- and q-axis currents, torque, and three-phase current waveform of PMSM are observed by oscilloscope.

The given initial speed of the motor is set as 60 r/min, and the load torque is set as 97.6 kNm. After the motor is stable, the given speed rises to 90 r/min at a certain moment. Then the given speed rises to 120 r/min at a certain moment after the motor is stable. The motor response curves of PMSM in the case of motor speed mutation are shown in Figure 7. It can be seen from Figure 7 that during the motor speed mutation, the motor speed with SVM-DTC and improved MPCC method can follow the reference speeds and stabilize at the given speed within 0.444 s and 0.436 s, respectively. The torque ripple with SVM-DTC and improved MPCC method under half load are less than 18.6% and 9.2%, and the three-phase current of improved MPCC method has better sinusoidal degree than of SVM-DTC.

The given initial speed of the motor is set as 120 r/min, and the load torque is set as 97.6 kNm. After the motor is stable, the load torque increases to rated load of 195.2 kNm at a certain moment. And the load torque drops to half load of 97.6 kNm at a certain moment after the motor is stable. The motor response curves of PMSM in the case of motor load mutation are shown in Figure 8. It can be seen from Figure 8 that when there is a sudden change in load during steady operation, the speed of SVM-DTC and improved MPCC method follows and stabilizes at the given speed of 120 r/min within

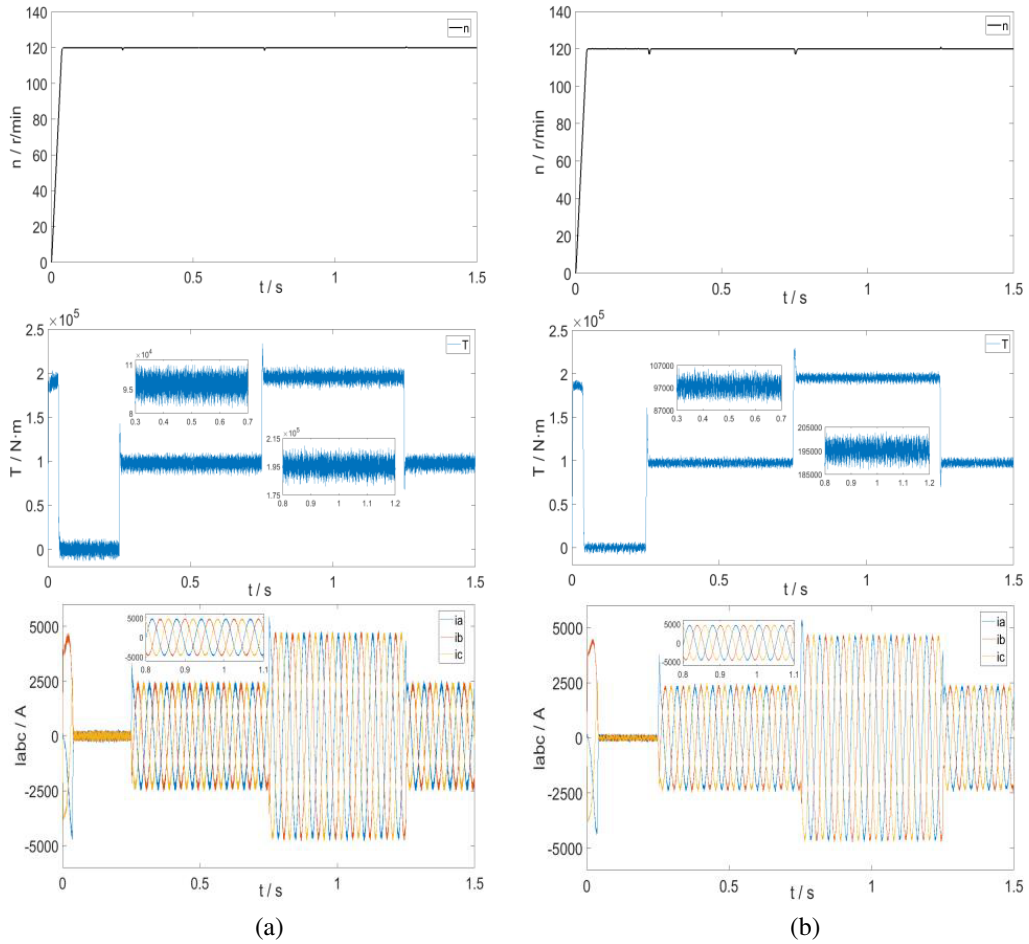

Figure 5. The motor response curves of the PMSM control system based on (a) SVM-DTC and (b) improved MPCC.

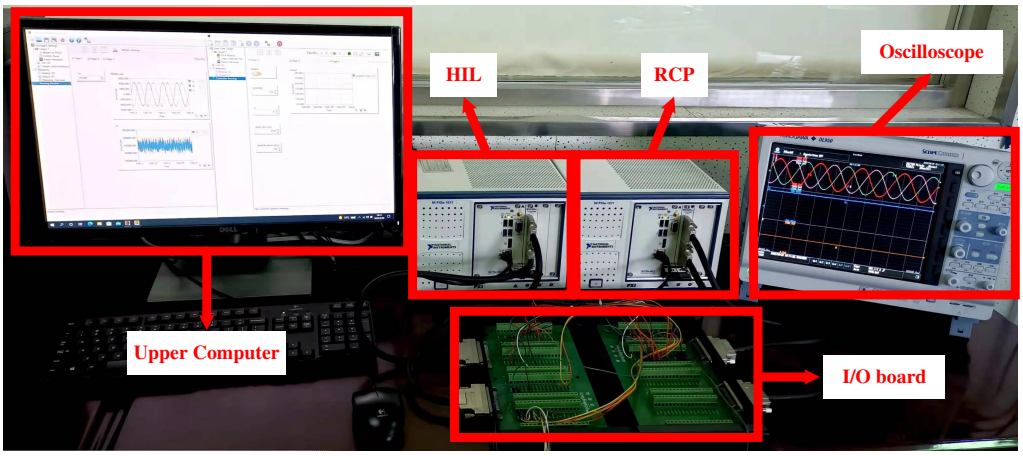

Figure 6. The experimental platform.

40 s and 8.45 s respectively. The torque ripple of SVM-DTC and improved MPCC method under rated load are less than 9.70% and 5.1%, respectively, and the three-phase current of improved MPCC method has better sinusoidal degree than of SVM-DTC.

It can be seen from Figure 7 to Figure 8 that when the given speed or the load of the PMSM control system for marine electric propulsion changes suddenly, the speed of the motor control system with the improved MPCC strategy can more quickly stabilize at the given speed than SVM-DTC strategy. And the torque ripple of the motor drive system with the improved MPCC strategy can be reduced by 9.4% and 4.8%, respectively, compared with SVM-DTC in the case of motor speed and torque variation.

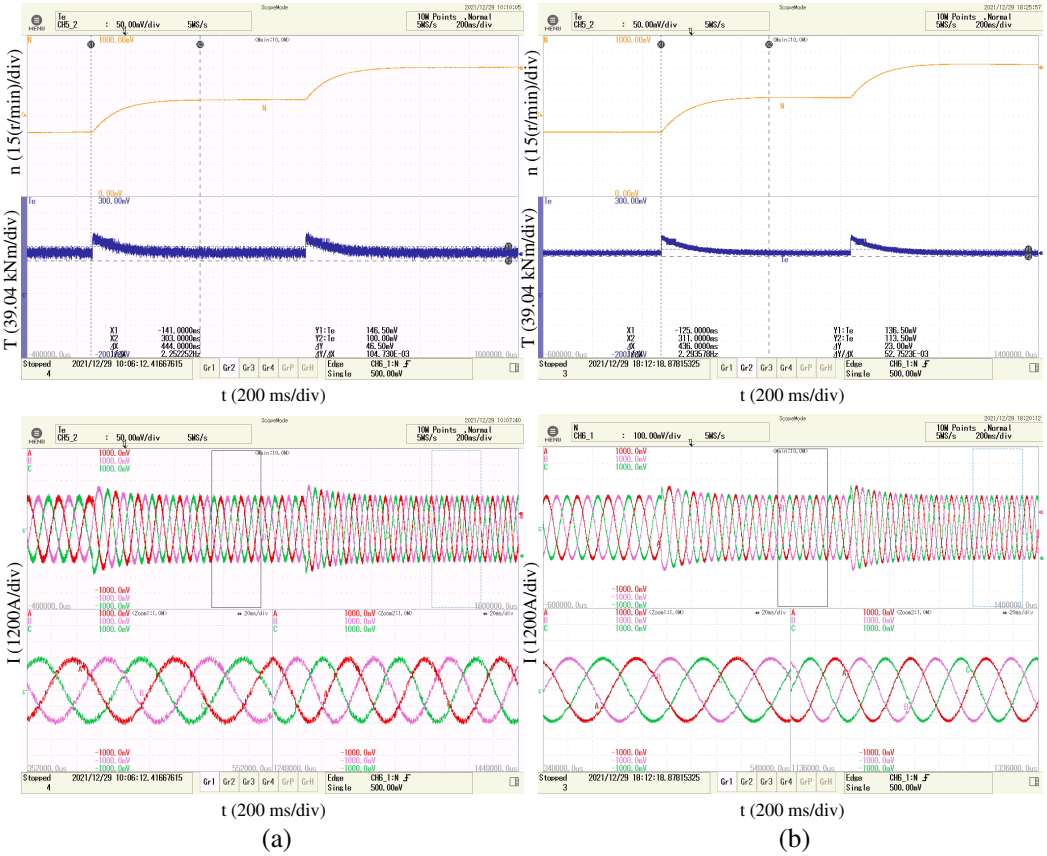

Figure 7. The motor response curves of PMSM in the case of motor speed mutation. (a) SVM-DTC. (b) Improved MPCC.

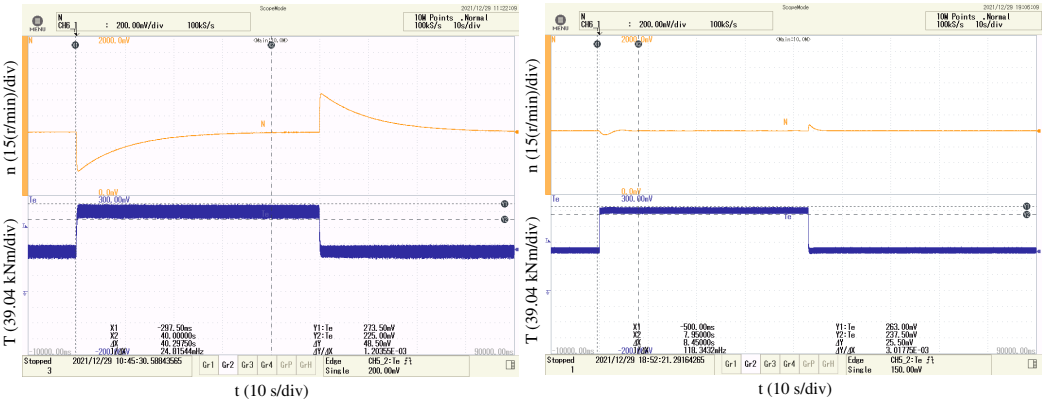

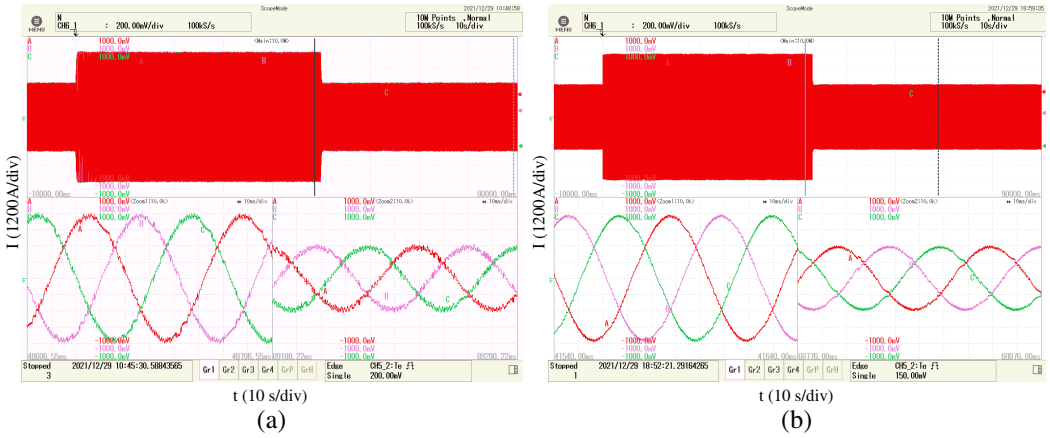

Figure 8. The motor response curves of PMSM in the case of motor load mutation. (a) SVM-DTC. (b) Improved MPCC.

6. CONCLUSIONS

In this paper, the proposed improved MPCC strategy of PMSM for marine electric propulsion is proposed based on the analysis of the mathematical model of PMSM in *d-q* coordinate system which can greatly reduce motor torque ripple and ensure the motor working more smoothly. The simulated and experimental results show that the torque ripple of improved MPCC strategy of PMSM proposed in this paper is significantly reduced compared with SVM-DTC of PMSM, and the steady-state performance is greatly improved. The proposed method has great significance to the further study of the control technology of PMSM for marine electric propulsion.

ACKNOWLEDGMENT

This work was supported by the National Natural Science Foundation of China under Project 51777024.

REFERENCES

1. Chandar, S. A. and S. K. Panda, "Detection and isolation of interturn faults in inductors of LCL filter for marine electric propulsion system," *IEEE Transactions on Transportation Electrification*, Vol. 4, No. 1, 232–248, 2018.
2. Wen, S., T. Zhao, Y. Tang, Y. Xu, M. Zhu, and Y. Huang, "A joint photovoltaic-dependent navigation routing and energy storage system sizing scheme for more efficient all-electric ships," *IEEE Transactions on Transportation Electrification*, Vol. 6, No. 3, 1279–1289, 2020.
3. Haxhiu, A., J. Kyyrä, R. Chan, and S. Kanerva, "Improved variable DC approach to minimize drivetrain losses in fuel cell marine power systems," *IEEE Transactions on Industry Applications*, Vol. 57, No. 1, 882–893, 2021.
4. Zhang, Z., H. Guo, Y. Liu, Q. Zhang, P. Zhu, and R. Iqbal, "An improved sensorless control strategy of ship IPMSM at full speed range," *IEEE Access*, Vol. 7, 178652–178661, 2019.
5. Ren, J., Y. Liu, N. Wang, et al., "Sensorless control of ship propulsion interior permanent magnet synchronous motor based on a new sliding mode observer," *ISA Transactions*, Vol. 54, No. 2, 15–26, 2015.
6. Ojaghlu, P. and A. Vahedi, "Specification and design of ring winding axial flux motor for rim-driven thruster of ship electric propulsion," *IEEE Transactions on Vehicular Technology*, Vol. 68, No. 2, 1318–1326, 2019.

7. Xu, X., X. Song, K. Wang, et al., "Modulation and voltage balancing control of dual five-level ANPC inverter for ship electric propulsion systems," *Chinese Journal of Electrical Engineering*, Vol. 7, No. 4, 78–92, 2021.
8. Amin, M. M., F. F. M. El-Sousy, O. A. Mohammed, G. A. A. Aziz, and K. Gaber, "MRAS-based super-twisting sliding-mode estimator combined with block control and DTC of six-phase induction motor for ship propulsion application," *IEEE Transactions on Industry Applications*, Vol. 57, No. 6, 6646–6658, 2021.
9. Jayaprakasan, S., S. Ashok, and R. Ramchand, "Current error space vector based hysteresis controller for VSI fed PMSM drive," *IEEE Transactions on Power Electronics*, Vol. 35, No. 10, 10690–10699, 2020.
10. Kim, J. S., S. Oh, and S. H. Kim, "A study on the speed and torque control of propulsion motor for electric propulsion ship by direct torque control," *Journal of Advanced Marine Engineering and Technology*, Vol. 33, No. 6, 946–951, 2009.
11. Zhang, X. and G. H. B. Foo, "A constant switching frequency-based direct torque control method for interior permanent-magnet synchronous motor drives," *IEEE Transactions on Mechatronics*, Vol. 21, No. 3, 1445–1456, 2016.
12. Cheema, M. A. M., J. E. Fletcher, D. Xiao, and M. F. Rahman, "A direct thrust control scheme for linear permanent magnet synchronous motor based on online duty ratio control," *IEEE Transactions on Power Electronics*, Vol. 31, No. 6, 4416–4428, 2016.
13. Naganathan, P. and S. Srinivas, "Direct torque control techniques of three-level H-bridge inverter fed induction motor for torque ripple reduction at low speed operations," *IEEE Transactions on Industrial Electronics*, Vol. 67, No. 10, 8262–8670, 2020.
14. Lakhimsetty, S., V. S. P. Satelli, R. S. Rathore, and V. T. Somasekhar, "Multilevel torque hysteresis-band based direct-torque control strategy for a three-level open-end winding induction motor drive for electric vehicle applications," *IEEE Journal of Emerging and Selected Topics in Power Electronics*, Vol. 7, No. 3, 1969–1981, 2019.
15. Sebtahmadi, S. S., H. Pirasteh, S. H. Aghay Kaboli, A. Radan, and S. Mekhilef, "A 12-sector space vector switching scheme for performance improvement of matrix-converter-based DTC of IM drive," *IEEE Transactions on Power Electronics*, Vol. 30, No. 7, 3804–3817, 2015.
16. Vinod, B. R., M. R. Baiju, and G. Shiny, "Five-level inverter-fed space vector based direct torque control of open-end winding induction motor drive," *IEEE Transactions on Energy Conversion*, Vol. 33, No. 3, 1392–1401, 2018.
17. Ananth, M. B. J., M. Vennila, and J. A. Thulasi, "A novel direct torque control scheme for induction machines with space vector modulation," *2016 International Conference on Electrical, Electronics, and Optimization Techniques (ICEEOT)*, 4773–4779, 2016.
18. Wang, Z., X. Wang, J. Cao, M. Cheng, and Y. Hu, "Direct torque control of T-NPC inverters-fed double-stator-winding PMSM drives with SVM," *IEEE Transactions on Power Electronics*, Vol. 33, No. 2, 1541–1553, 2018.
19. Moati, Y., K. Kouzi, and A. Iqbal, "Adaptive optimized DTC-SVM using metaheuristic bat algorithm for DSIM fed by IMC based on robust synergetic speed controller," *International Transactions on Electrical Energy Systems*, Vol. 31, No. 1, 1–25, 2021.
20. Luo, P., H. Zhao, C. Guo, and S. Cheng, "Model predictive control of permanent magnet synchronous propulsion motor applied in USV with composite ship-propeller load," *2018 Eighth International Conference on Information Science and Technology (ICIST)*, 212–217, 2018.
21. Liu, C., Z. Pan, J. Wang, H. Fan, W. Yang, and H. Zhang, "Development of distributed photovoltaic grid-connected simulation system based on StarSim platform," *2020 IEEE 3rd Student Conference on Electrical Machines and Systems (SCEMS)*, 843–846, 2020.
22. Xiang, J., J. Xu, H. Wang, C. Li, G. Cui, and Y. Peng, "Reconfigurable line-side converter for DC voltage matching and ripple suppression in multisystem locomotives," *IEEE Transactions on Power Electronics*, Vol. 36, No. 5, 5832–5844, 2021.